

# Design and Implementation of Smell Agent Optimizer for Parameters Estimation of Single and Double Diode in PV System: A Comparative Analysis

Mohamed F. Elnaggar<sup>a,b,1,\*</sup>

<sup>a</sup> Department of Electrical Engineering, College of Engineering, Prince Sattam Bin Abdulaziz University, Al-Kharj 11942, Saudi Arabia

<sup>b</sup> Department of Electrical Power and Machines Engineering, Faculty of Engineering, Helwan University, Helwan 11795, Egypt

<sup>1</sup> [mfelnaggar@yahoo.com](mailto:mfelnaggar@yahoo.com)

\* Corresponding Author

## ARTICLE INFO

## ABSTRACT

### Article history

Received May 23, 2024

Revised July 07, 2024

Accepted July 26, 2024

### Keywords

Nonlinear Optimization;  
Single-Diode PV Model;  
Two-Diode PV Model;  
MATLAB Simulation;  
Green Energy

One of the most important and desirable options for moving toward clean electric energy sources is solar energy. Therefore, a PV system's characteristics play a significant role in determining how effective it is across a range of temperature and radiation scenarios. One can consider the PV model's parameter estimation to be a nonlinear optimization situation. This work makes use of a novel application of the smell agent optimizer (SAO) created to forecast the undefined parameters of the PV model's single- and two-diode equivalent circuits. The goal of this effort is to create an accurate photovoltaic model that can accurately represent its performance under variable operating conditions. The square of the mean squared error between the actual measured curve and the current-voltage curve derived from the model defines the intended objective function. The suggested system is constructed and tested experimentally in a range of temperature and light conditions. Next, the MATLAB software is used to create the simulated PV model integrated with the SAO. The PV parameters are then predicted by comparing the experimental data with the convergence of the SAO based on the PV model. Based on the observed properties, the suggested approach for determining the parameters of an actual solar cell has been put into practice and contrasted with eight other optimization techniques. The outstanding efficacy of the method utilized compared with alternate methods is demonstrated by the statistical comparison of the ideal objective function resulting from the difference in the current-voltage curve produced from the optimized circuit model and the measurement.

This is an open-access article under the [CC-BY-SA](https://creativecommons.org/licenses/by-sa/4.0/) license.



## 1. Introduction

Recently, renewable energy sources such as solar and wind energy have been highly utilized in different applications, either stand-alone or grid-connected, as a result of their features of sustainability, low working costs, and zero pollution production [1], [2]. Solar energy is considered the most renewable energy widespread in various places over the world. PV panels are characterized by a shortened installation period, uncomplicated design, noisiness, and long operation life [3]-[6].

The singular solar cell (SC) produces only a mean voltage of 0.5-0.65 V [7]. For the generation of a higher effective voltage, it has become necessary to bind several SCs in series to build a single module [8]-[10]. Adding numerous modules in series and parallel can increase V and I, respectively; this arrangement of several modules has formed an array [11]. There are three key points in PV datasheets relating to the I/V relationship of the PV system in ordinary atmospheric conditions. This includes produced voltage at no-load ( $V_{nl}$ ), current at short circuit ( $I_{sc}$ ), as well as voltage ( $V_{mp}$ ) and current ( $I_{mp}$ ) with maximum generated power ( $P_{max}$ ). Nevertheless, these aforementioned points are not enough to describe such PV systems for further studies. In reality, these conditions alter continuously. To ensure a satisfactory performance analysis of PV systems under various operating conditions, SCs, modules, and arrays must always have a correct I/V relationship. SCs' I/V characteristics can be predicted using two familiar models, namely the one-diode and two-diode models (ODM and TDM), respectively. To define ODM efficiently, five uncertain parameters must be defined, including diode ideality factor, photo-generated current, saturation current, series resistance, and shunt resistance, TDM also requires seven unknown parameters. Moreover, there is a triple diode model that can be employed to model PV models. This model involves nine unknown parameters. Still, both ODM and TDM have been given special attention in the current study [12]-[14].

Modeling and simulating the behavior of PV system components, including SCs, is essential in the design or analysis phase of PV systems. In general, the simulation of PV systems includes two stages of mathematical modeling and formulation and then the estimation of model parameters. ODM and TDM models are usually used to model SCs. After choosing the desired model, to obtain the necessary parameters, one must use the characteristics of the SC provided by the manufacturers in their catalog. The basic characteristic used to estimate the parameters of the solar cell model is their I-V curve, which is obtained practically and by measuring in the laboratory under certain conditions. In ODM and TDM models, there are 5 and 7 unknown parameters, respectively, which should be estimated as accurately as possible [15], [16]. Because the modeling error in one SC, due to their very large number in a PV system and especially in high-capacity power plants, will lead to a significant error in the modeling of the entire system. Therefore, one of the main challenges in modeling solar cells is an accurate and appropriate estimation of their equivalent circuit parameters [17]-[19]. The current methods used to estimate these parameters are divided into two categories: analytical methods and numerical methods. In analytical methods, generally, the information included in the product catalog, such as  $V_{nl}$ ,  $I_{sc}$ , maximum power point (MPP) voltage, and MPP current, is used to obtain the I-V characteristic [20]-[22]. The implementation of these methods is easier, but their accuracy depends a lot on the initial points selected in the algorithm, and in some cases, they do not converge to a suitable solution. To overcome the problems of analytical methods, researchers use numerical methods in which all the measured points in the I-V curve are used, and as a result, the obtained solution will be reliable and valid. Numerical methods include two deterministic and meta-heuristic methods. In the deterministic method, classic optimization methods such as iterative curve fitting [23], Newton-Raphson method [24], and Lambert W-function [25] are used. Using the deterministic approach in optimization problems brings limitations such as differentiability and convexity of the objective function. On the other hand, the next drawback of these methods is high sensitivity to initial values and getting trapped in locally optimal solutions.

In the past few decades, the use of meta-heuristic algorithms (MHAs) in engineering applications and problems has become very popular among researchers. MHAs have also been used in estimating the equivalent circuit parameters of SCs [26]. Most of the methods based on probabilistic and population-based MHA are modeled on the behavior of nature. In these methods, there is no need to establish the condition of convexity, continuity, and differentiability of the objective functions (OFs) [27], and therefore, these methods have found various applications in solving engineering problems, including the estimation of SC parameters. Several studies have attempted to determine the PV model parameters using various optimization strategies. Mainly genetic algorithms [28], particle swarm optimization (PSO) [29], harmony search (HS) [30],

simulated annealing (SA) [31], artificial immune system (AIS) [32], differential evolution (DE) [33], cat swarm optimization (CSO) [34], and artificial bee colony (ABC) [35].

Other recent heuristic-based optimizers include the enhanced leader PSO [36], forensic-based investigation algorithm [37], slime mold optimizer (SMO) [38], cuckoo search algorithm (CSA) [39], bird matting optimizer (BMO) [40], coyote approach [41], chaos PSO (CPSO) [42], grey wolf optimizer (GWO) [43], and generalized oppositional teaching learning based optimization (GOTLBO) [44] are employed to estimate the PV model ambiguous parameters. Other algorithms, in addition to the ones mentioned above, have been used to define the PV model parameters, including the chaotic whale optimization algorithm (CWOA) [45], bonobo optimizer (BO) [46], whippy harris hawks optimization (WHHO) [47], adaptive differential evolution algorithm [48], flower pollination algorithm [49], chaotic gradient-based optimizer (CGBO) [50], and ions motion optimization (IMO) [51].

The main challenges are the problem of estimating the parameters of SCs, identifying and choosing or providing an optimization algorithm with high search capability, and ensuring the appropriate scanning of the problem space to avoid local optima and achieve greater accuracy. Therefore, these techniques still need to be adjusted to determine the best optimum value for various PV modules. The best method for determining the optimal value of PV parameters has yet to be discovered. In this study, the first objective is setting up the experimental test bed PV system to extract the practical results at different operational conditions. The second objective is utilizing the recent optimization algorithm smell agent optimizer (SAO) in cooperation with the MATLAB program and based on practical results for precise identification of PV parameters. The performance and effectiveness of the utilized algorithm will be examined under various working conditions. In this research, the parameter estimation based on the measured curve of an SC for both ODM and TDM models is implemented with the new SAO, and its results are compared with the PSO, DE, SA, HS, TLBO, ABC, CSO, and BBO algorithms which for the same SC is applied under the same conditions and compared statistically under the same conditions. The statistical comparison, along with the examination of the convergence graphs in the same conditions shows the better and more reliable performance of the used method and also proves the necessity of using more accurate and reliable methods in solving the problem of estimating the parameters of the SC model.

## 2. Equivalent Circuit of SCs with ODM and TDM Models

The equivalent SCs can be expressed as is in Fig. 1. The corresponding mathematical model is then described in Eq. (1) to Eq. (5). The outputted current can then be expressed in function for all parameters and variables that appear in Fig. 1. Equivalent circuit model of a TDM solar cell shown in Fig. 2.

The total current that moves in the SC is expressed in Eq. (1), and the diode current that can be exposed is presented as it is in Eq. (2). The diode voltage is then exposed as it is in Eq. (3), and the SC voltage can be exposed in the function of temperature constant as it is in Eq. (4). Finally, the total current outputted from the SC is like it is in Eq. (5). If the double diode model is used for simulating the SC comportment, then the corresponding mathematical model is as it is in Eq. (6) [13], [52]-[54].

$$I = I_{PV} - I_D - I_P \quad (1)$$

$$I_D = I_{SD} \left[ e^{\left( \frac{V_D}{\alpha V_t} \right)} - 1 \right] \quad (2)$$

$$V_D = V + R_S I \quad (3)$$

$$V_t = \frac{kT}{q} \quad (4)$$

$$I = I_{PV} - I_{SD} \left[ e^{\left( \frac{V+R_S I}{\alpha_1 V_t} \right)} - 1 \right] - \frac{V + R_S I}{R_P} \quad (5)$$

$$I = I_{PV} - I_{D1} - I_{D2} - I_P = I_{PV} - I_{SD1} \left[ e^{\left( \frac{V+R_S I}{\alpha_1 V_t} \right)} - 1 \right] - I_{SD2} \left[ e^{\left( \frac{V+R_S I}{\alpha_2 V_t} \right)} - 1 \right] - \frac{V + R_S I}{R_P} \quad (6)$$

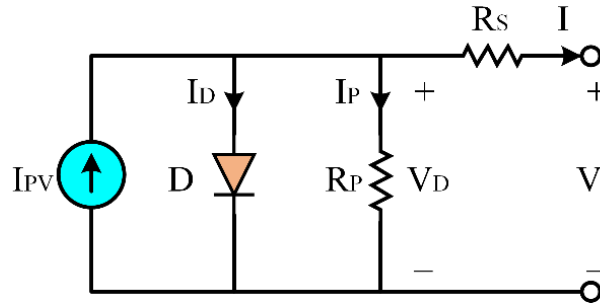


Fig. 1. Equivalent circuit model of an ODM solar cell

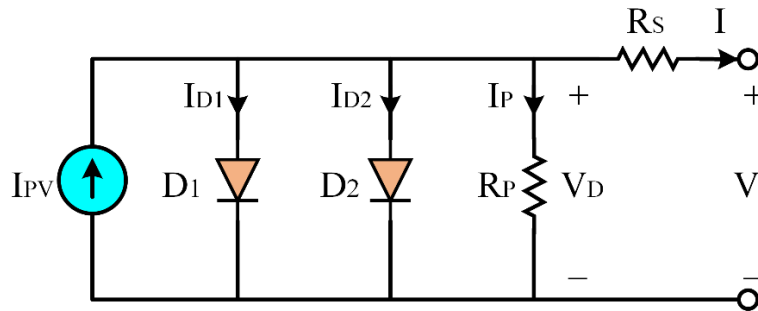


Fig. 2. Equivalent circuit model of a TDM solar cell

If the ODM is selected, the determining parameters are  $\alpha$ ,  $R_P$ ,  $R_S$ ,  $I_{SD}$ ,  $I_{PV}$ ; however, if the TDM is selected, the determining parameters  $\alpha_1$ ,  $\alpha_2$ ,  $R_P$ ,  $R_S$ ,  $I_{SD1}$ ,  $I_{SD2}$ ,  $I_{PV}$ . Determining the parameters of an ODM for a PV system is a crucial step in understanding its behavior and optimizing its performance. The ODM is widely used to represent the electrical characteristics of an SC or module, capturing the complex relationship between  $I$ ,  $V$ , and the surrounding environmental conditions. The parameters of this model include the ideality factor, the series and shunt resistances, the saturation current, and the light-generated current. To determine these parameters, a variety of methods can be employed, such as curve fitting techniques, iterative algorithms, or experimental measurements under controlled conditions. These approaches involve analyzing the  $I$ - $V$  and  $P$ - $V$  curves of the PV system, taking into account factors like temperature, irradiance, and SC/module configuration. By accurately determining the parameters of the ODM, engineers and researchers can gain valuable insights into the PV system's performance, predict its behavior under different operating conditions, and devise strategies to enhance its overall efficiency and reliability.

However, the TDM accounts for the complex behavior of the SC or module, considering both recombination and shunt effects that can significantly impact its performance. The parameters of this model include the ideality factors, the series and shunt resistances, the saturation currents, and the light-generated currents for both diodes. To determine these parameters, various techniques can be utilized, such as nonlinear regression analysis, optimization algorithms, or experimental measurements using specialized test setups. These methods involve analyzing the  $I$ - $V$  and  $P$ - $V$  curves of the PV system under different operating conditions, including variations in temperature, irradiance, and load. By accurately determining the parameters of the TDM, researchers and engineers can gain a deeper understanding of the PV system's behavior, predict its performance under diverse scenarios, and develop strategies to enhance its efficiency and reliability. This comprehensive

modeling approach enables more precise system design, optimization, and control, thereby facilitating the advancement of solar energy technologies. For all these conditions and specifications, the optimization tool will be used to resolve this optimization problem.

### 3. Formulation and Problem-Solving Method

The design in Fig. 3, shows the overall process and explains where the algorithm will be implemented for doing the parameter estimation.

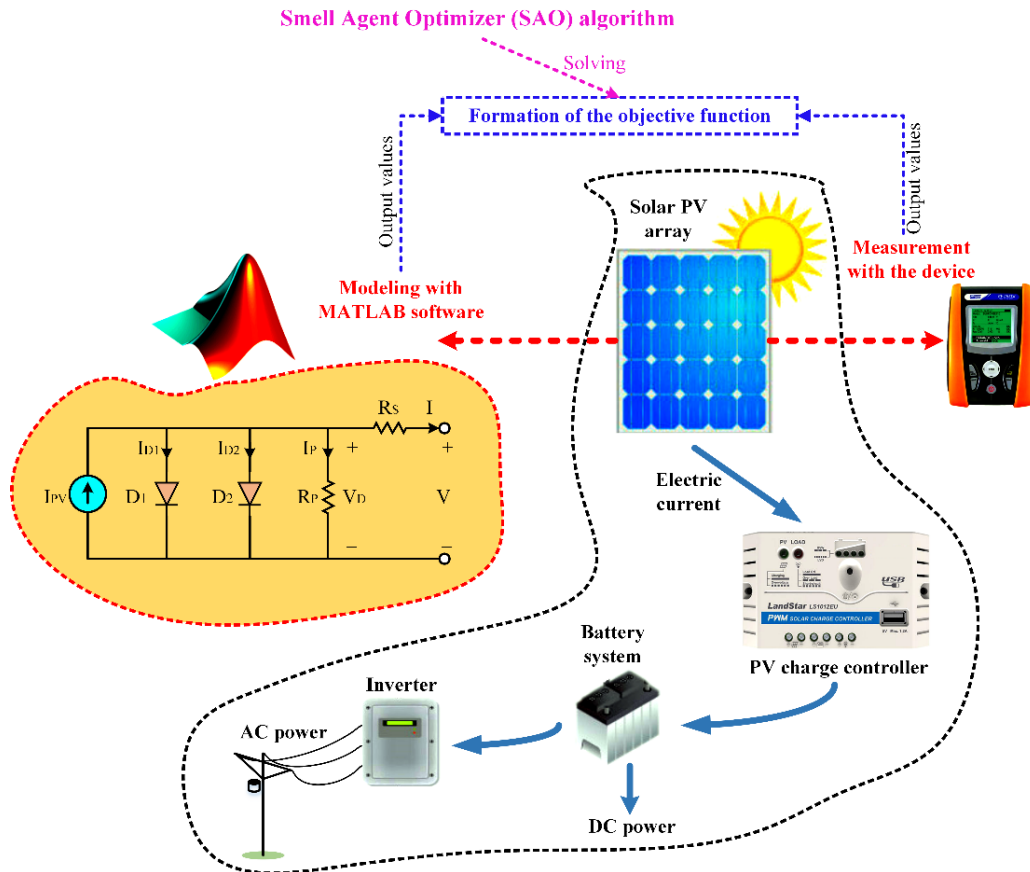


Fig. 3. Overview of the proposed structure of PV parameter estimation

The OF consists of the difference between the modeled  $I_{mdl}(x)$  and measured ( $I_{msrd}$ ) values based on root mean square error (RMSE).

$$F(x) = \sqrt{\frac{1}{N} \sum_{i=1}^N (I_{mdl}(x) - I_{msrd})^2} \tag{7}$$

The vector variables for ODM are  $x = [IPV, IsD, \alpha, RS, RP]$

The vector variables for TDM are  $x = [IPV, IsD1, IsD2, \alpha1, \alpha2, RS, RP]$

### 4. Applied SAO Algorithm

The SAO is an innovative and nature-inspired optimization technique that draws inspiration from the olfactory system of the behavior of insects such as ants and the ability to communicate. To optimize the problems, SAO was designed and developed as a metaheuristic algorithm, SAO is adjusted to solve complex optimization problems and does not impose a significant computational

burden by mimicking the behavior of agents that navigate their environment using smell as their guiding sense [55]-[57].

SAO is a stochastic search technique that uses a population or swarm of individual elements where animals detect and follow the scent of food or other attractive sources. Each animal shows an independent achievement solution to a problem and adjusts its own flying experience in the boundary space to find the optimal solution. The agents converge towards favorable areas of the solution space by iteratively modifying and improving their positions based on the strength and direction of the encountered odors [55], [57].

These agents generate and release “smell” in the form of candidate solutions, which diffuse through the search space and attract other agents. By iteratively updating and improving their positions based on the intensity and direction of the encountered smells, the agents converge toward promising regions of the solution space. SAO's ability to exploit the principles of smell-guided navigation makes it a powerful and efficient optimization algorithm applicable to a wide range of real-world problems. Three essential steps define the SAO function [55], [57].

#### 4.1. Sniffing Mode

Sniffing mode is often used in the initial stages of optimization processing to gather information about the landscape and to generate a diverse set of candidate solutions. The idea of sniffing mode on the ability of a smell agent. As a result, the agent decides to move towards the direction of the smell molecules or move away from the smell molecules. The concept of agent is represented by a position particle and the velocity vector as follows [55], [57]:

$$X_i^n = [x_{i1}, x_{i2}, x_{i3} \dots x_{in}] \quad (8)$$

$$V_i^n = [v_{i1}, v_{i2}, \dots v_{in}] \quad (9)$$

where  $i$  is the particle number, and  $n = (1, 2, 3, \dots, N)$  is the iteration number. The agent determined the positions of particles with the best and worst sniffing fitness, respectively.

#### 4.2. Trailing Mode

Once the sniffing mode completes processing, the agent instinctively follows racks the molecule's journey and tracks the trail position part of the smell molecules until its source is identified. As a result, the agent should now sniff the smell of every molecule, which was evaluated where initial velocity and position are updated. However, the agent constrained only the optimal one in the search process as follows [55], [57]:

$$X_i^{n+1} = X_{id}^n + V_{id}^{n+1} \quad (10)$$

#### 4.3. Modeling Assumptions

To create the mathematical model of the SAO, the following presumptions were made [55], [57].

- Although each agent has a unique smell capacity, the agents all react to odorant molecules in the same way.
- The smell molecules are not attracted to one another.
- Every molecule has its unique concentration smell, even if they have more than one smell. Therefore, the smell molecules continuously evaporate from the smell source in the agent's direction.
- In comparison with velocity of the smell agent, the evaporation of the smell molecule was negligible.

The flowchart of the optimization process of the SAO algorithm is shown in Fig. 4.

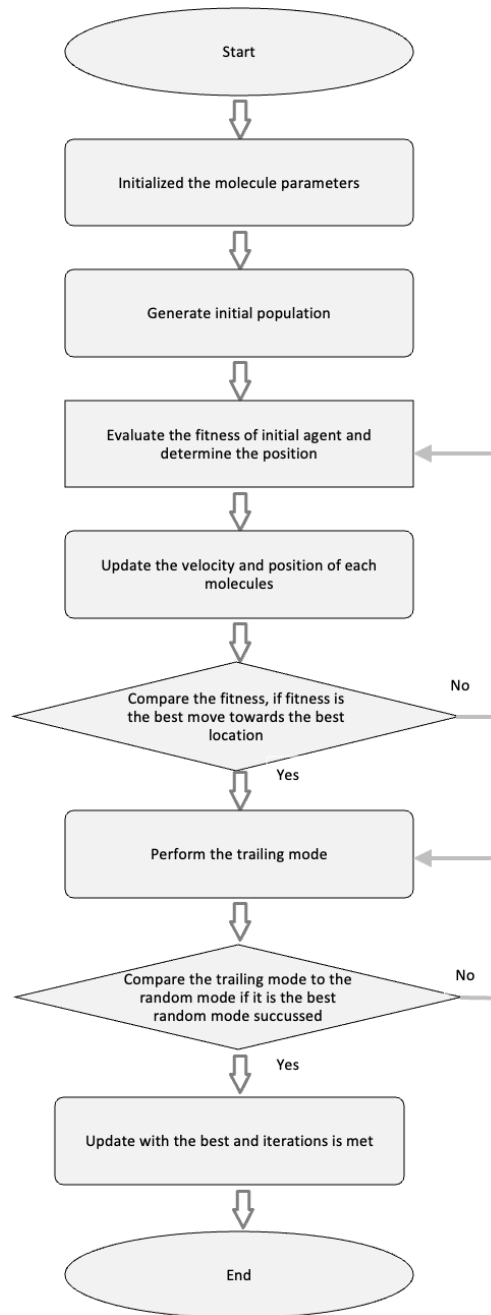


**Fig. 4.** Overview of the algorithm flowchart

Initially, all parameters that prerequisites, such as the position and the velocity of the smell molecules, are initialized in the algorithm. Next, the initial iterative optimization process begins randomly, and the position and the velocity of the molecules are updated every iteration. The movement of each molecule within the search space is calculated according to a given performance function that assesses the fitness of the molecules. In the next step, the position of each molecule can be changed based on its own local best solution. After that, evaluate the fitness of the sniffing mode and update the position of the agent with the position of a molecule having the best sniffing fitness with the best position of molecules. Then, the process continues, and the best fitness is retained while the worst fitness is discarded through greedy selection. Until the predefined number of iterations is met. The process is also terminated when predefined stopping criteria are satisfied, or no significant improvement is achieved over many iterations.

## 5. Simulation Results

To estimate the parameters of the SC model, the measured I-V characteristic of the SC is needed. The SC considered in this article is a commercial R.T.C France silicon SC with a diameter of 57 mm. The characteristics of this SC include 26 pairs of current and voltage numbers at a temperature of 33 °C and radiation of 1000 W/m<sup>2</sup> [46]. The upper and lower limit values of the parameters for the ODM and TDM models are considered as follows [36]:

$$ODM: l = [0, 0, 1, 0, 0]$$

$$u = [1, 0, 2, 0.5, 100]$$

$$TDM: l = [0, 0, 0, 1, 1, 0, 0]$$

$$u = [1, 10 - 6, 10 - 6, 2, 2, 0.5, 100]$$

In optimization, three important factors are  $E^{worst}$ ,  $E^{best}$ , and  $k_{max}$ , which respectively indicate the number of elements produced with the worst fit value, the number of particles produced with the best quality of fit, and the maximum number of generations considered in the optimization process. Here, the adjustment parameters of the SAO are limited to these three factors, and based on the best solutions obtained in different iterations,  $E^{best} = 20$ ,  $E^{worst} = 0$ , and  $k_{max} = 100$  are obtained. The solution of the SAO has been compared with the results of 8 other algorithms including PSO [29], HS [30], SA [31], DE [33], CSO [34], ABC [35], TLBO [44], and BBO [58] to make an appropriate evaluation of the new method. The parameters of these algorithms have been applied based on the suggested settings in the relevant references and an attempt has been made to find the best solution as much as possible. Also, to compare the performance of the algorithms fairly, the number of iterations, the population in each iteration, and other involved parameters are set in such a way that each algorithm executes the objective function a maximum of 50,000 times during the optimization process. The execution of each algorithm was also repeated 25 times to provide an appropriate statistical analysis of their outputs.

### 5.1. ODM and TDM Model Results

The statistical results of optimization, including the minimum, median, mean, maximum, and standard deviation of the RMSE value for the ODM model of the SC, are shown in Table 1. In Table 1, the accuracy of each algorithm can be evaluated and compared. Among the above indicators, the values of standard deviation express the reliability of each algorithm in obtaining the optimal solution in different iterations. The comparison of the values in Table 1 shows that the SAO has the best performance based on all the indicators, especially the standard deviation, with a difference. Also, SAO has the most reliability in terms of the difference in the optimal output solution in each run. DE, ABC, and PSO methods also provide suitable minimum solutions, but their median, average, maximum, and expressly standard deviation indices are far from the performance of the SAO.

To better compare the performance of the used algorithms, the convergence curve is used to estimate the parameters of the ODM model is shown in Fig. 5. As is shown, the SAO has a better convergence performance in the same number of evaluations of the objective function and has converged to the optimal solution earlier in all numbers with the same number of iterations. The statistical results of optimization similar to ODM mode for the TDM model are shown in Table 2. Comparing the values in Table 2 shows that the SAO has the best performance based on all the indicators. Also, due to the standard deviation being much less than other algorithms, SAO has the highest reliability in terms of the difference in the optimal output solution every time it is executed. DE, TLBO, and HS methods also provide minimum suitable solutions compared to other methods, but their mean, median, maximum, and especially standard deviation indices are far from the results of the SAO.

It is worth mentioning that, in general, the RMSE values in the TDM model are higher in most cases compared to the ODM model. The reason for this is the addition of two parameters and another nonlinear function to the problem. Especially since these two parameters are effective in the nonlinear part of the model (or the diode) and make the estimation problem more difficult. Another

advantage of the SAO is that the minimum and median value of RMSE in the TDM is lower compared to the ODM, while the performance of other algorithms has dropped in the TDM, except for the minimum in the DE algorithm. The convergence curve of all algorithms used to estimate TDM parameters is shown in Fig. 6. As is shown, the SAO has a better convergence performance in the same number of evaluations of the objective function. The superiority of the SAO is more evident in Fig. 6 compared to Fig. 5, and in the lower number of iterations, the distance of the optimal solution of this method is much greater compared to other methods.

**Table 1.** RMSE statistical results are obtained from different algorithms for the ODM model

Algorithm	Minimum	Median	Mean	Maximum	Standard deviation
PSO [29]	$9.87146 \times 10^{-4}$	$1.02892 \times 10^{-3}$	$1.05433 \times 10^{-3}$	$1.19436 \times 10^{-3}$	$6.14225 \times 10^{-5}$
HS [30]	$1.02934 \times 10^{-3}$	$1.41752 \times 10^{-3}$	$1.40162 \times 10^{-3}$	$1.58762 \times 10^{-3}$	$1.41871 \times 10^{-4}$
SA [31]	$1.09761 \times 10^{-3}$	$1.84634 \times 10^{-3}$	$1.79256 \times 10^{-3}$	$2.86389 \times 10^{-3}$	$6.09843 \times 10^{-4}$
DE [33]	$9.78731 \times 10^{-4}$	$1.41132 \times 10^{-3}$	$1.47278 \times 10^{-3}$	$1.84312 \times 10^{-3}$	$2.75341 \times 10^{-4}$
CSO [34]	$1.87712 \times 10^{-3}$	$4.04351 \times 10^{-3}$	$8.01189 \times 10^{-3}$	$4.47735 \times 10^{-2}$	$1.41341 \times 10^{-2}$
ABC [35]	$9.78118 \times 10^{-4}$	$1.07712 \times 10^{-3}$	$1.12241 \times 10^{-3}$	$1.31872 \times 10^{-3}$	$1.11987 \times 10^{-4}$
TLBO [44]	$9.87273 \times 10^{-4}$	$1.10441 \times 10^{-3}$	$1.02114 \times 10^{-3}$	$1.14315 \times 10^{-3}$	$5.71388 \times 10^{-5}$
BBO [58]	$9.87431 \times 10^{-4}$	$1.50841 \times 10^{-3}$	$1.48352 \times 10^{-3}$	$2.18762 \times 10^{-3}$	$3.85681 \times 10^{-4}$
SAO	$9.75041 \times 10^{-4}$	$9.75041 \times 10^{-4}$	$9.75041 \times 10^{-4}$	$9.75043 \times 10^{-4}$	$1.87357 \times 10^{-9}$

**Table 2.** RMSE statistical results are obtained from different algorithms for the TDM model

Algorithm	Minimum	Median	Mean	Maximum	Standard deviation
PSO [29]	$1.09881 \times 10^{-3}$	$1.38379 \times 10^{-3}$	$1.47756 \times 10^{-3}$	$2.19432 \times 10^{-3}$	$2.78643 \times 10^{-4}$
HS [30]	$1.10448 \times 10^{-3}$	$1.52431 \times 10^{-3}$	$1.37871 \times 10^{-3}$	$2.19457 \times 10^{-3}$	$2.43873 \times 10^{-4}$
SA [31]	$1.37631 \times 10^{-3}$	$2.46211 \times 10^{-3}$	$2.52671 \times 10^{-3}$	$3.72761 \times 10^{-3}$	$5.67342 \times 10^{-4}$
DE [33]	$9.86437 \times 10^{-4}$	$1.19781 \times 10^{-3}$	$1.21461 \times 10^{-3}$	$2.03276 \times 10^{-3}$	$2.52761 \times 10^{-4}$
CSO [34]	$2.28176 \times 10^{-3}$	$6.47543 \times 10^{-3}$	$6.01145 \times 10^{-3}$	$8.47641 \times 10^{-3}$	$8.11961 \times 10^{-3}$
ABC [35]	$1.10675 \times 10^{-3}$	$1.10435 \times 10^{-3}$	$1.15367 \times 10^{-3}$	$1.54311 \times 10^{-3}$	$6.14743 \times 10^{-4}$
TLBO [44]	$1.01734 \times 10^{-3}$	$1.10442 \times 10^{-3}$	$1.15742 \times 10^{-3}$	$1.56581 \times 10^{-3}$	$1.56614 \times 10^{-4}$
BBO [58]	$1.22941 \times 10^{-3}$	$2.13765 \times 10^{-3}$	$2.39976 \times 10^{-3}$	$3.23651 \times 10^{-3}$	$9.14671 \times 10^{-4}$
SAO	$9.72746 \times 10^{-4}$	$9.72723 \times 10^{-4}$	$9.75251 \times 10^{-4}$	$9.77614 \times 10^{-4}$	$2.43571 \times 10^{-4}$

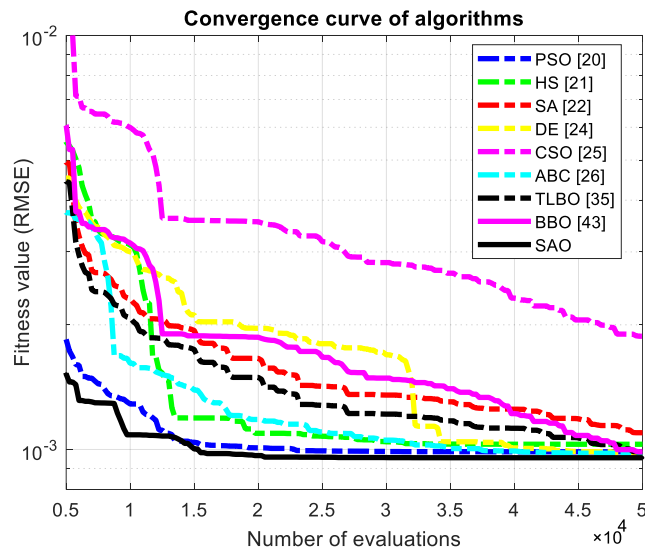


**Fig. 5.** Convergence curve of different algorithms for the ODM model

The parameters of the model in the best solution of each algorithm are presented in Table 3 and Table 4. In Table 3, the parameters of  $I_{PV}$ ,  $\alpha$ , and  $R_s$  are obtained to some extent close to each other, but the difference of other parameters in different algorithms is significant. In Table 4, with the addition of two other parameters, only  $I_{PV}$  and  $R_s$  have a small difference in different algorithms, and other parameters are far apart in comparison with different algorithms. Even the overall difference of the optimal parameters obtained in the DE, which provided the best solution among

other algorithms after the SAO, is very significant with the SAO. This issue shows the challenge of the existence of many local optima in the problem search space and the importance of appropriate search in the used algorithm and avoiding local optima, especially in the TDM model.

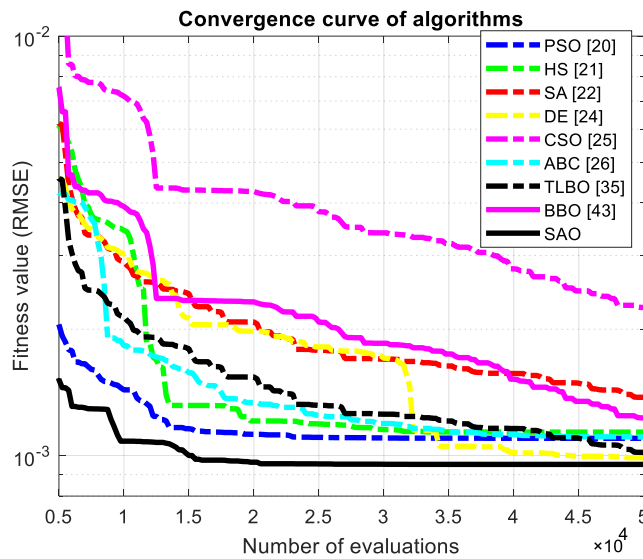


Fig. 6. Convergence curve of different algorithms for the TDM model

Table 3. Estimated parameters for the ODM model by different algorithms

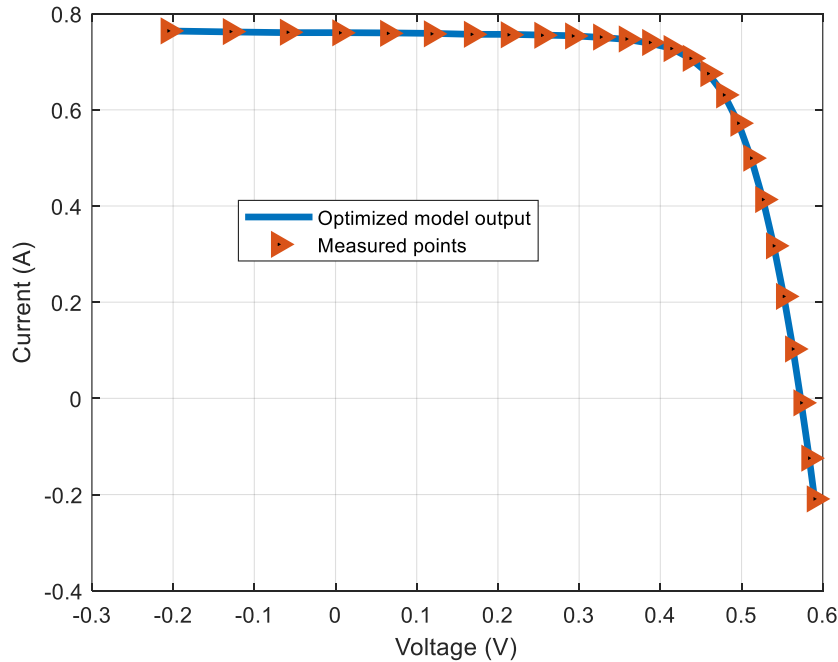
Algorithm	$I_{pv}$ (A)	$I_{SD}$ ( $\mu$ A)	$\alpha$	$R_s$ ( $\Omega$ )	$R_p$ ( $\Omega$ )
PSO [29]	0.76062	0.33414	1.48446	0.03626	55.03412
HS [30]	0.76061	0.41856	1.49575	0.03531	63.58872
SA [31]	0.76138	0.33681	1.48571	0.03612	49.50272
DE [33]	0.76088	0.31868	1.48002	0.03635	53.35951
CSO [34]	0.76065	0.36103	1.50227	0.03511	89.85637
ABC [35]	0.76081	0.34017	1.49332	0.03617	56.21632
TLBO [44]	0.76079	0.33014	1.47941	0.03592	54.12121
BBO [58]	0.76075	0.33503	1.49047	0.03641	63.84881
SAO	0.76077	0.32301	1.48117	0.03636	54.65936

Table 4. Estimated parameters for the TDM model by different algorithms

Algorithm	$I_{pv}$ (A)	$I_{SD1}$ ( $\mu$ A)	$I_{SD2}$ ( $\mu$ A)	$\alpha_1$	$\alpha_2$	$R_s$ ( $\Omega$ )	$R_p$ ( $\Omega$ )
PSO [29]	0.76014	0.01232	0.32517	1.67884	1.47974	0.03609	52.39113
HS [30]	0.76037	0.18114	0.32558	1.71884	1.48562	0.03603	64.80515
SA [31]	0.76203	0.32712	0.00414	1.48243	1.87113	0.03601	44.58683
DE [33]	0.76057	0.34154	0.00573	1.49111	1.97421	0.03615	55.51014
CSO [34]	0.76204	0.03031	0.49841	1.68913	1.53243	0.03517	89.85637
ABC [35]	0.76058	0.15132	0.23743	1.70517	1.51275	0.03637	56.21632
TLBO [44]	0.76103	0.30246	0.14011	1.46974	1.99042	0.03648	54.12087
BBO [58]	0.76056	0.13847	0.37884	1.45117	1.58952	0.03527	63.84881
SAO	0.76078	0.33846	0.27869	1.99527	1.46879	0.03648	54.65926

Also, to evaluate the best solution, the I-V and P-V characteristics of the SC obtained from the optimized model with the SAO, along with the measured points, are shown in Fig. 7 and Fig. 8, respectively. The very good matching of the output characteristics of the model and the measurement points in these figures indicates the very good performance of the SAO. Therefore, the better performance of the SAO for estimating the parameters of the SC model in both ODM and TDM models is proven. The accuracy of two optimized models, ODM and TDM, is shown in Fig. 9. The accuracy of both models is lower at high voltages and higher at low voltages. Also, the TDM model is more accurate at low voltages. Another interesting point is the drop in the accuracy of the model

after passing the MPP. Of course, the accuracy of the model in general and, especially around the MPP, is very suitable, and it is sufficient for engineering applications and analysis of PV systems.



**Fig. 7.** Comparative characteristic in the TDM model: optimized model output with the measurement data

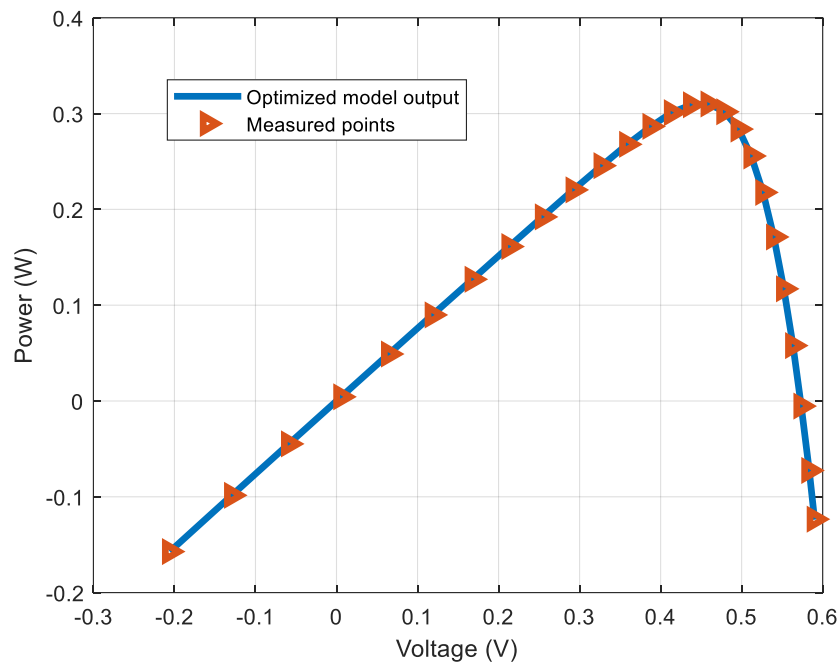


**Fig. 8.** Comparative characteristic in the TDM model: optimized model output with the measurement data

## 5.2. Implementation of the Effect of Temperature and Radiation on SC Performance

SC panels perform better at low temperatures than at high temperatures. The power produced by the SC panel at low temperatures is much higher than at high temperatures. It should be noted that with the increase in temperature, the current changes are insignificant, which can be assumed to be constant, but the output voltage will decrease significantly, and as a result, the output power of the SC panel will decrease. Therefore, to reach the I-V characteristic, as well as the P-V under different

temperature and radiation conditions, the I-V characteristic can be defined in terms of temperature and radiation as Eq. (11). In which  $\alpha G = G/G_{ref}$  and K is the temperature correction factor [59].

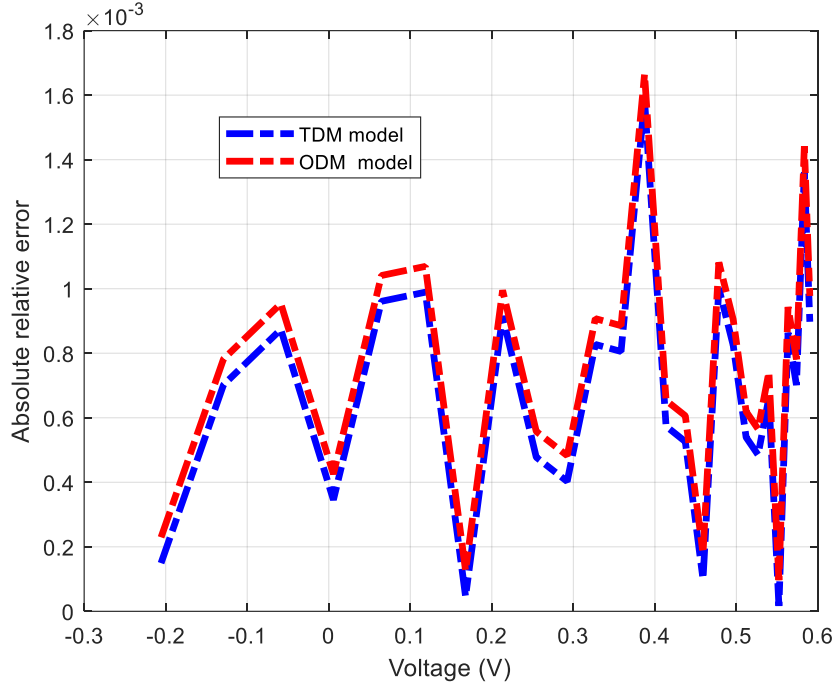


**Fig. 9.** Comparison of the accuracy of ODM and TDM models

$$I(\alpha_G, T) = \alpha_G I_{PV}(T) - I_{SD}(\alpha_G, T) \left[ e^{\left( \frac{\alpha_G [V + KI(T - T_{ref})] + R_S I}{\alpha_G n T} \right)} - 1 \right] - \frac{\alpha_G [V + KI(T - T_{ref})] + R_S I}{\alpha_G R_P} \quad (11)$$

$$I_{PV}(T) = I_{PV,ref} + \mu_{Isc}(T - T_{ref}) \quad (12)$$

$$I_{SD}(\alpha_G, T) = \alpha_G \left[ \frac{I_{PV}(T) - V_{oc}(\alpha_G, T)/R_P}{e^{V_{oc}(\alpha_G, T)/nT} - 1} \right] \quad (13)$$

$$V_{oc}(\alpha_G, T) = V_{oc,ref} + nT \ln(\alpha_G) + \mu_{Voc}(T - T_{ref}) \quad (14)$$

$$I_{sc}(\alpha_G, T) = I_{sc,ref} \cdot \alpha_G + \mu_{Isc}(T - T_{ref}) \quad (15)$$

Here,  $n$  is the coefficient of the ideality of the diode,  $T$  is the temperature,  $\mu_{Isc}$  is the temperature coefficient of the short circuit current, and  $\mu_{Voc}$  is the temperature coefficient of the open circuit voltage. To show the effect of temperature on the output power of the solar panel, an experimental test has been carried out. Fig. 10 shows a 245 W panel installed on the roof of the electrical engineering college of Azad University, Bushehr branch which has been the cooling of the SC panel has been done to understand the effect of temperature on the performance of the SC panel. As it is shown, to cool the SC panel, the space behind the panel is completely covered with spiral tubes, and the passage of water through it cools the panel. In addition, by using a PV-CHECKS measuring device, the amount of radiation, the temperature of the PV panel, the changes in  $I$  and  $V$ , and the changes in the power of the panel are measured at any moment.

Now, at an ambient temperature of 34°C, a comparison has been made between the power output from the panel in normal mode and cooling mode. Table 5 shows the results of this comparison for the amount of radiation of 960 W/m<sup>2</sup>. For a better understanding, the effect of temperature on voltage

and power output from the panel is shown in Fig. 11. As can be seen, when the temperature of the panel was lowered to 14°C, the output power of the SC panel increased by 10%.

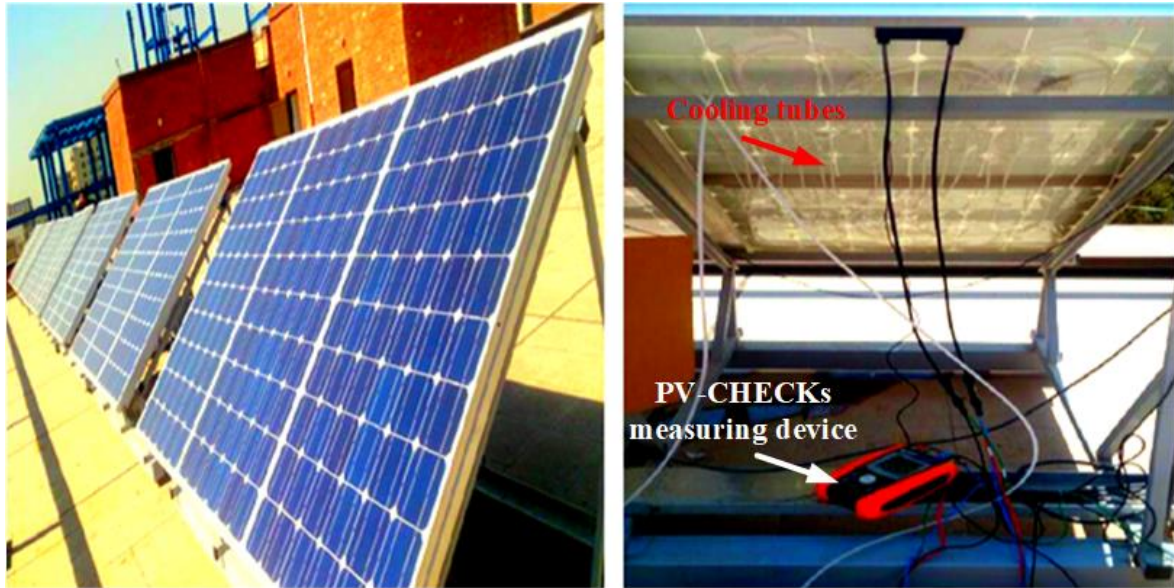


Fig. 10. Back and front view of 245 W panel

Table 5. Effect of temperature on the output power of the SC panel

Mode of operation	Amount of radiation (W/m <sup>2</sup> )	Panel temperature (°C)	Panel output power (W)
Without cooling	960	60	184
With cooling	960	46	201

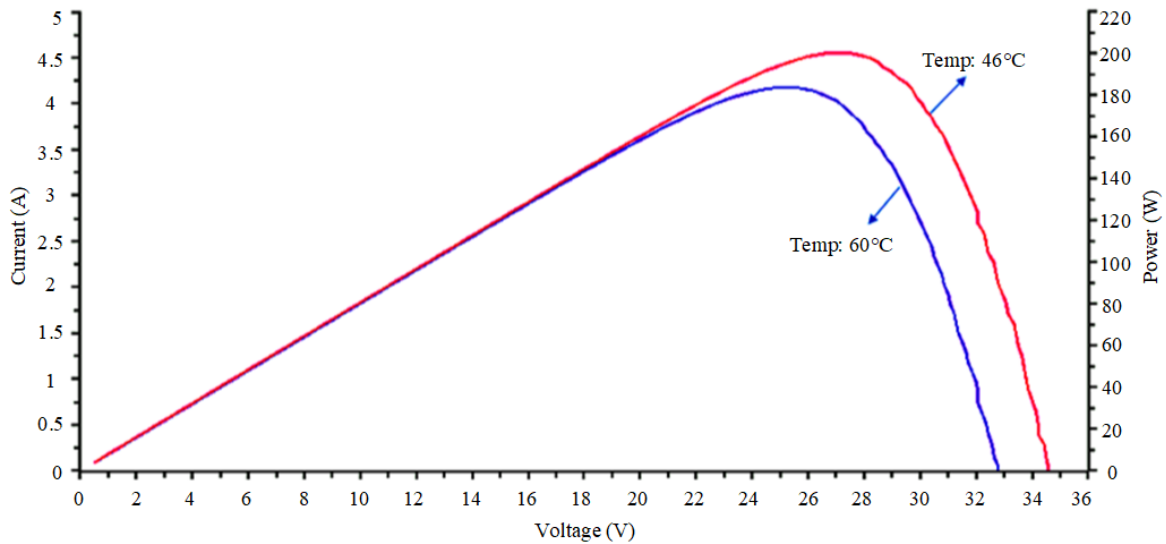


Fig. 11. The comparative curve of the effect of temperature on the voltage and output power of the panel

In the following, the performance of the SAO algorithm in estimating PV module parameters under the influence of temperature and radiation changes is evaluated. Table 6 shows the specifications of the PV module according to the catalog information. Fig. 12 and Fig. 13 show the performance of the SAO in modeling the optimal PV output with the points measured by the device, respectively, for the I-V and P-V characteristics for different radiations at a temperature of 25°C. Similarly, the mentioned characteristics at different temperatures for 1000 W/m<sup>2</sup> radiation are shown in Fig. 14 and Fig. 15. As it is shown, with the increase of radiation, the maximum power produced

by the module increases, which, according to Eq. 11 and Eq. 12, is due to the increase of open circuit voltage and short circuit current. Also, with the increase in temperature, the maximum output power of the module will decrease. This is because with the increase in temperature, although according to Eq.12, the short circuit current increases slightly, the significant decrease in the open circuit voltage, according to Eq. 11 causes a decrease in the output power (in this case  $\mu_{Isc} > 0$  and  $\mu_{Voc} < 0$ ).

**Table 6.** Specifications of the PV module under study

Type (Kyocera)	$V_{mp}$	$I_{mp}$	$P_{max}$	$V_{oc}$	$I_{sc}$
KD240GX-LFB2	29.8	8.06	240.188	36.9	8.59

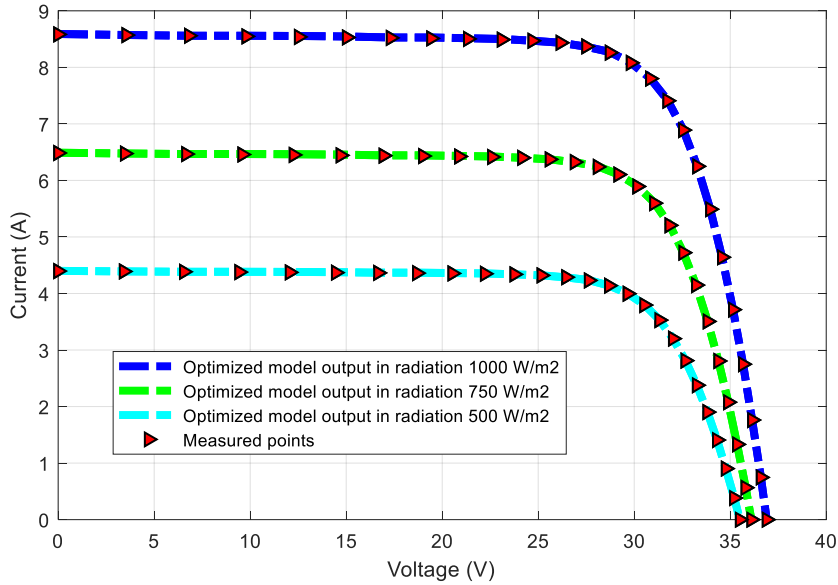


**Fig. 12.** I-V characteristic under different radiations at 25°C

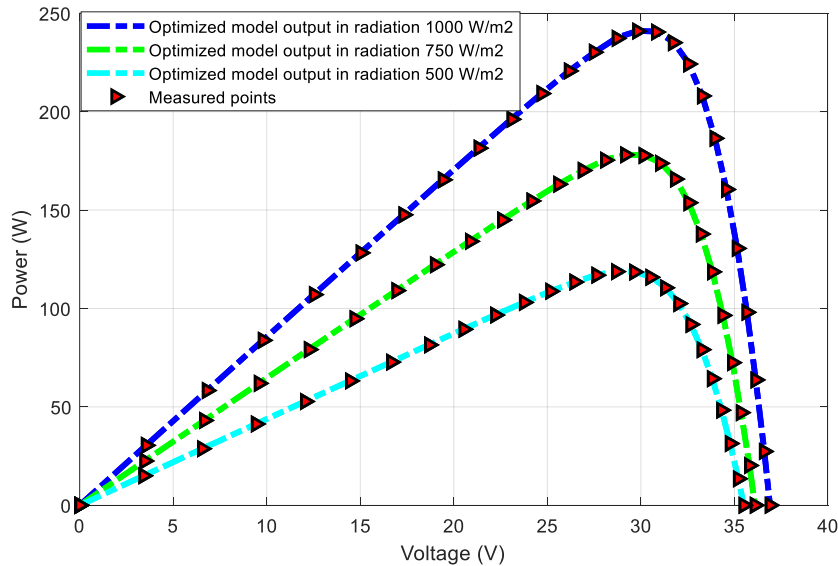


**Fig. 13.** P-V characteristic under different radiations at 25°C

As is shown from the performance of the SAO, by matching the output of the optimized model with the measured points, the values of the PV module parameters have been estimated with better accuracy under various conditions. Finally, Table 7 shows the parameter values estimated by the SAO.

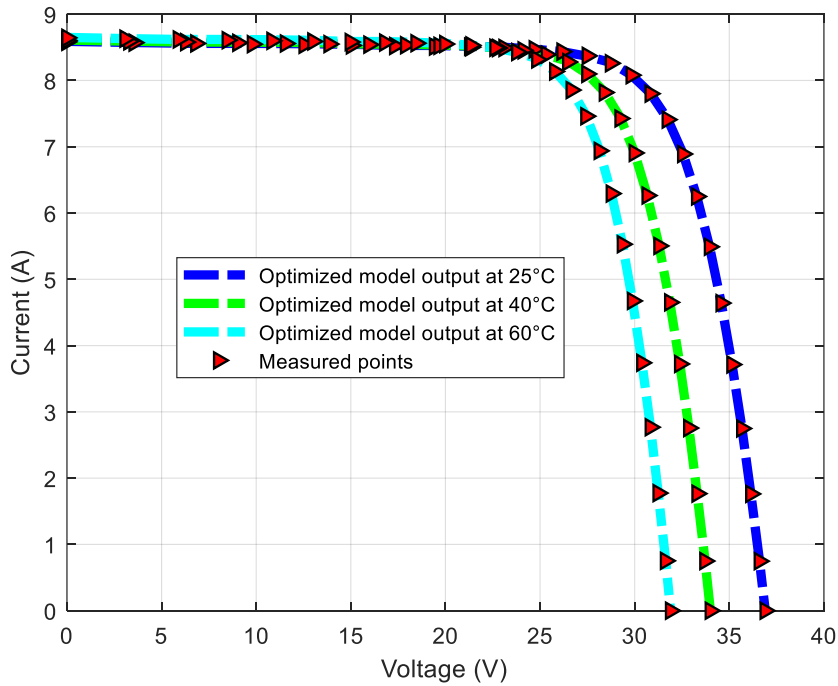


Fig. 14. I-V characteristic under different temperatures in 1000 W/m<sup>2</sup> radiation

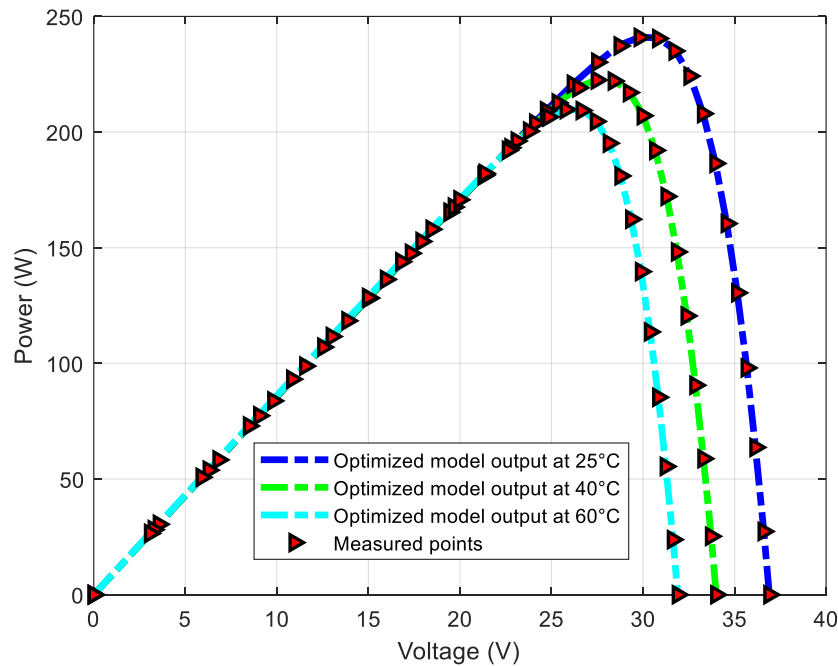


Fig. 15. P-V characteristic under different temperatures in 1000 W/m<sup>2</sup> radiation

Table 7. Values of estimated PV module parameters

Type (Kyocera)	$I_{PV}$	$I_{SD}$	$R_s$	$R_p$	$n$	$P_{max}$ (Calculated)
KD240GX-LFB2	8.6134	$3.22 \times 10^{-11}$	0.3485	129.9159	0.0047	240.179

## 6. Conclusion

The smell agent optimization algorithm is used to help define the PV system parameters in variable conditions. This is the objective of this study, and the efficiency of the proposed solution is

shown in the given results by making a comparison with more than six other optimization methods. The test was made for a variable radiation form and variable temperature conditions, as it is known that the PV temperature is extremely variable due to the location of the overall PV generator. The given results have demonstrated a perfect estimation for the PV parameters, and this can help secure the panels from any future problems that can happen. More applications can be attached to this study in future endeavors and maybe testing more optimization tools can make the study more interesting to the researchers.

**Author Contribution:** All authors contributed equally to the main contributor to this paper. All authors read and approved the final paper.

**Funding:** The authors extend their appreciation to Prince Sattam bin Abdulaziz University for funding this research work through the project number (PSAU/2024/01/29320).

**Data Availability:** The data used to support the findings of this study are available at reasonable request from the corresponding author.

**Acknowledgment:** The authors extend their appreciation to Prince Sattam bin Abdulaziz University for funding this research work through the project number (PSAU/2024/01/29320).

**Conflicts of Interest:** The authors declare that they have no conflicts of interest.

## References

- [1] M. Awad *et al.*, "A review of water electrolysis for green hydrogen generation considering PV/wind/hybrid/hydropower/geothermal/tidal and wave/biogas energy systems, economic analysis, and its application," *Alexandria Engineering Journal*, vol. 87, pp. 213–239, 2024, <https://doi.org/10.1016/j.aej.2023.12.032>.
- [2] M. M. Mahmoud, "Improved current control loops in wind side converter with the support of wild horse optimizer for enhancing the dynamic performance of PMSG-based wind generation system," *International Journal of Modelling and Simulation*, vol. 43, no. 6, pp. 952-966, 2023, <https://doi.org/10.1080/02286203.2022.2139128>.
- [3] O. M. Lamine *et al.*, "A Combination of INC and Fuzzy Logic-Based Variable Step Size for Enhancing MPPT of PV Systems," *International Journal of Robotics and Control Systems*, vol. 4, no. 2, pp. 877-892, 2024, <https://doi.org/10.31763/ijrcs.v4i2.1428>.
- [4] R. Kassem *et al.*, "A Techno-Economic-Environmental Feasibility Study of Residential Solar Photovoltaic / Biomass Power Generation for Rural Electrification : A Real Case Study," *Sustainability*, vol. 16, no. 5, p. 2036, 2024, <https://doi.org/10.3390/su16052036>.
- [5] R. Benkercha, S. Moulahoum, and B. Taghezouit, "Extraction of the PV modules parameters with MPP estimation using the modified flower algorithm," *Renewable Energy*, vol. 143, pp. 1698-1709, 2019, <https://doi.org/10.1016/j.renene.2019.05.107>.
- [6] N. F. Ibrahim *et al.*, "A new adaptive MPPT technique using an improved INC algorithm supported by fuzzy self-tuning controller for a grid-linked photovoltaic system," *PLoS One*, vol. 18, no. 11, p. e0293613, 2023, <https://doi.org/10.1371/journal.pone.0293613>.
- [7] A. A. Tarabsheh, M. Akmal, and M. Ghazal, "Series connected photovoltaic cells-Modelling and analysis," *Sustainability*, vol. 9, no. 3, p. 371, 2017, <https://doi.org/10.3390/su9030371>.
- [8] V. P. Gantasala, "Solar augmentation of power plants in the UAE," *Applied Solar Energy*, vol. 52, pp. 271-277, 2016, <https://doi.org/10.3103/S0003701X16040095>.
- [9] S. H. Hakmi, "Applications of Multi-Objective OPF Solutions with Optimal Placement of Multiple and Multi-Type FACTS Units to IEEE System: Comparison of Different Approaches," *International Journal of Robotics and Control Systems*, vol. 4, no. 3, pp. 1075-1091, 2024, <https://doi.org/10.31763/ijrcs.v4i3.1472>
- [10] B. S. Atia *et al.*, "Applications of Kepler Algorithm-Based Controller for DC Chopper: Towards

- Stabilizing Wind Driven PMSGs under Nonstandard Voltages,” *Sustainability*, vol. 16, no. 7, p. 2952, 2024, <https://doi.org/10.3390/su16072952>.
- [11] W. Yang, R. R. Prabhakar, J. Tan, S. D. Tilley, and J. Moon, “Strategies for enhancing the photocurrent, photovoltage, and stability of photoelectrodes for photoelectrochemical water splitting,” *Chemical Society Reviews*, vol. 48, no. 19, pp. 4979-5015, 2019, <https://doi.org/10.1039/C8CS00997J>.
- [12] F. Menzri, T. Boutabba, I. Benlaloui, H. Bawayan, M. I. Mosaad, and M. M. Mahmoud, “Applications of hybrid SMC and FLC for augmentation of MPPT method in a wind-PV-battery configuration,” *Wind Engineering*, 2024, <https://doi.org/10.1177/0309524X241254364>.
- [13] N. F. Ibrahim *et al.*, “Operation of Grid-Connected PV System With ANN-Based MPPT and an Optimized LCL Filter Using GRG Algorithm for Enhanced Power Quality,” *IEEE Access*, vol. 11, pp. 106859-106876, 2023, <https://doi.org/10.1109/ACCESS.2023.3317980>.
- [14] N. F. Ibrahim *et al.*, “Multiport Converter Utility Interface with a High-Frequency Link for Interfacing Clean Energy Sources (PV\Wind\Fuel Cell) and Battery to the Power System: Application of the HHA Algorithm,” *Sustainability*, vol. 15, no. 18, p. 13716, 2023, <https://doi.org/10.3390/su151813716>.
- [15] A. H. Elmetwaly *et al.*, “Modeling, Simulation, and Experimental Validation of a Novel MPPT for Hybrid Renewable Sources Integrated with UPQC: An Application of Jellyfish Search Optimizer,” *Sustainability*, vol. 15, no. 6, p. 5209, 2023, <https://doi.org/10.3390/su15065209>.
- [16] O. M. Kamel, A. A. Z. Diab, M. M. Mahmoud, A. S. Al-Sumaiti, and H. M. Sultan, “Performance Enhancement of an Islanded Microgrid with the Support of Electrical Vehicle and STATCOM Systems,” *Energies*, vol. 16, no. 4, p. 1577, 2023, <https://doi.org/10.3390/en16041577>.
- [17] A. Gholami, M. Ameri, M. Zandi, and R. Gavagsaz Ghoachani, “A single-diode model for photovoltaic panels in variable environmental conditions: Investigating dust impacts with experimental evaluation,” *Sustainable Energy Technologies and Assessments*, vol. 47, p. 101392, 2021, <https://doi.org/10.1016/j.seta.2021.101392>.
- [18] A. K. Podder, K. Ahmed, N. K. Roy and M. Habibullah, “Design and Simulation of a Photovoltaic and Fuel Cell Based Micro-grid System,” *2019 International Conference on Energy and Power Engineering (ICEPE)*, pp. 1-6, 2019, <https://doi.org/10.1109/CEPE.2019.8726694>.
- [19] A. Gholami, M. Ameri, M. Zandi, R. Gavagsaz Ghoachani, and M. Gholami, “A fast and precise double-diode model for predicting photovoltaic panel electrical behavior in variable environmental conditions,” *International Journal of Ambient Energy*, vol. 44, no. 1, pp. 1298-1315, 2023, <https://doi.org/10.1080/01430750.2023.2173290>.
- [20] M. Khurshed *et al.*, “Review of Flower Pollination Algorithm: Applications and Variants,” *2020 International Conference on Engineering and Emerging Technologies (ICEET)*, pp. 1-6, 2020, <https://doi.org/10.1109/ICEET48479.2020.9048215>.
- [21] M. Dashtdar and M. Dashtdar, “Voltage-Frequency Control (v-f) of Islanded Microgrid Based on Battery and MPPT Control,” *American Journal of Electrical and Computer Engineering*, vol. 4, no. 2, pp. 35-48, 2020, <https://doi.org/10.11648/j.ajece.20200402.12>.
- [22] J. P. Ram, T. S. Babu, T. Dragicevic, and N. Rajasekar, “A new hybrid bee pollinator flower pollination algorithm for solar PV parameter estimation,” *Energy Conversion and Management*, vol. 135, pp. 463-476, 2017, <https://doi.org/10.1016/j.enconman.2016.12.082>.
- [23] L. Sandrolini, M. Artioli, and U. Reggiani, “Numerical method for the extraction of photovoltaic module double-diode model parameters through cluster analysis,” *Applied Energy*, vol. 87, no. 2, pp. 442-451, 2010, <https://doi.org/10.1016/j.apenergy.2009.07.022>.
- [24] C. Kumar and D. M. Mary, “Parameter estimation of three-diode solar photovoltaic model using an Improved-African Vultures optimization algorithm with Newton-Raphson method,” *Journal of Computational Electronics*, vol. 20, pp. 2563-2593, 2021, <https://doi.org/10.1007/s10825-021-01812-6>.
- [25] M. T. Benmessaoud, P. Vasant, A. B. Stambouli, and M. Tioursi, “Modeling and parameters extraction of photovoltaic cell and modules using the genetic algorithms with lambert W-function as objective function,” *Intelligent Decision Technologies*, vol. 14, no. 2, pp. 143-151, 2020, <https://doi.org/10.3233/IDT-180015>.

- [26] J. Ma, Z. Bi, T. O. Ting, S. Hao, and W. Hao, "Comparative performance on photovoltaic model parameter identification via bio-inspired algorithms," *Solar Energy*, vol. 132, pp. 606-616, 2016, <https://doi.org/10.1016/j.solener.2016.03.033>.
- [27] A. R. Jordehi, "Time varying acceleration coefficients particle swarm optimisation (TVACPSO): A new optimisation algorithm for estimating parameters of PV cells and modules," *Energy Conversion and Management*, vol. 129, pp. 262-274, 2016, <https://doi.org/10.1016/j.enconman.2016.09.085>.
- [28] N. Hamid, R. Abounacer, M. Idali Oumhand, M. Feddaoui, and D. Agliz, "Parameters identification of photovoltaic solar cells and module using the genetic algorithm with convex combination crossover," *International Journal of Ambient Energy*, vol. 40, no. 5, pp. 517-524, 2019, <https://doi.org/10.1080/01430750.2017.1421577>.
- [29] M. Merchaoui, A. Sakly, and M. F. Mimouni, "Particle swarm optimisation with adaptive mutation strategy for photovoltaic solar cell/module parameter extraction," *Energy Conversion and Management*, vol. 175, pp. 151-163, 2018, <https://doi.org/10.1016/j.enconman.2018.08.081>.
- [30] A. Askarzadeh and A. Rezaadeh, "Parameter identification for solar cell models using harmony search-based algorithms," *Solar Energy*, vol. 86, no. 11, pp. 3241-3249, 2012, <https://doi.org/10.1016/j.solener.2012.08.018>.
- [31] R. Bendaoud *et al.*, "New method for extracting physical parameters of PV generators combining an implemented genetic algorithm and the simulated annealing algorithm," *Solar Energy*, vol. 194, pp. 239-247, 2019, <https://doi.org/10.1016/j.solener.2019.10.040>.
- [32] B. Jacob, K. Balasubramanian, T. S. Babu and N. Rajasekar, "Parameter extraction of solar PV double diode model using artificial immune system," *2015 IEEE International Conference on Signal Processing, Informatics, Communication and Energy Systems (SPICES)*, pp. 1-5, 2015, <https://doi.org/10.1109/SPICES.2015.7091390>.
- [33] S. Li, Q. Gu, W. Gong, and B. Ning, "An enhanced adaptive differential evolution algorithm for parameter extraction of photovoltaic models," *Energy Conversion and Management*, vol. 205, p. 112443, 2020, <https://doi.org/10.1016/j.enconman.2019.112443>.
- [34] L. Guo, Z. Meng, Y. Sun, and L. Wang, "Parameter identification and sensitivity analysis of solar cell models with cat swarm optimization algorithm," *Energy Conversion and Management*, vol. 108, pp. 520-528, 2016, <https://doi.org/10.1016/j.enconman.2015.11.041>.
- [35] L. Xu, L. Bai, H. Bao and J. Jiang, "Parameter Identification of Solar Cell Model Based on Improved Artificial Bee Colony Algorithm," *2021 13th International Conference on Advanced Computational Intelligence (ICACI)*, pp. 239-244, 2021, <https://doi.org/10.1109/ICACI52617.2021.9435902>.
- [36] A. R. Jordehi, "Enhanced leader particle swarm optimisation (ELPSO): An efficient algorithm for parameter estimation of photovoltaic (PV) cells and modules," *Solar Energy*, vol. 159, pp. 78-87, 2018, <https://doi.org/10.1016/j.solener.2017.10.063>.
- [37] A. M. Shaheen, A. R. Ginidi, R. A. El-Sehiemy and S. S. M. Ghoneim, "A Forensic-Based Investigation Algorithm for Parameter Extraction of Solar Cell Models," *IEEE Access*, vol. 9, pp. 1-20, 2021, <https://doi.org/10.1109/ACCESS.2020.3046536>.
- [38] C. Kumar, T. D. Raj, M. Premkumar, and T. D. Raj, "A new stochastic slime mould optimization algorithm for the estimation of solar photovoltaic cell parameters," *Optik*, vol. 223, p. 165277, 2020, <https://doi.org/10.1016/j.ijleo.2020.165277>.
- [39] X. Chen and K. Yu, "Hybridizing cuckoo search algorithm with biogeography-based optimization for estimating photovoltaic model parameters," *Solar Energy*, vol. 180, pp. 192-206, 2019, <https://doi.org/10.1016/j.solener.2019.01.025>.
- [40] A. Askarzadeh and A. Rezaadeh, "Extraction of maximum power point in solar cells using bird mating optimizer-based parameters identification approach," *Solar Energy*, vol. 90, pp. 123-133, 2013, <https://doi.org/10.1016/j.solener.2013.01.010>.
- [41] A. A. Z. Diab, H. M. Sultan, T. D. Do, O. M. Kamel and M. A. Mossa, "Coyote Optimization Algorithm for Parameters Estimation of Various Models of Solar Cells and PV Modules," *IEEE Access*, vol. 8, pp. 111102-111140, 2020, <https://doi.org/10.1109/ACCESS.2020.3000770>.

- [42] A. T. Kiani, M. Faisal Nadeem, A. Ahmed, I. A. Sajjad, A. Raza and I. A. Khan, "Chaotic Inertia Weight Particle Swarm Optimization (CIWPSO): An Efficient Technique for Solar Cell Parameter Estimation," *2020 3rd International Conference on Computing, Mathematics and Engineering Technologies (iCoMET)*, pp. 1-6, 2020, <https://doi.org/10.1109/iCoMET48670.2020.9074085>.
- [43] A. Vinod and A. K. Sinha, "Estimation of parameters for one diode solar PV cell using grey Wolf optimizer to obtain exact V-I characteristics," *Journal of Engineering Research*, vol. 7, no. 1, pp. 1-19, 2019, <https://kuwaitjournals.org/jer/index.php/JER/article/view/4223>.
- [44] X. Chen, K. Yu, W. Du, W. Zhao, and G. Liu, "Parameters identification of solar cell models using generalized oppositional teaching learning based optimization," *Energy*, vol. 99, pp. 170-180, 2016, <https://doi.org/10.1016/j.energy.2016.01.052>.
- [45] J. Zhao, D. Zhang, Q. He, and L. Li, "A Hybrid-Strategy-Improved Dragonfly Algorithm for the Parameter Identification of an SDM," *Sustainability*, vol. 15, no. 15, p. 11791, 2023, <https://doi.org/10.3390/su151511791>.
- [46] A. A. Al-Shamma'a *et al.*, "Parameter estimation of photovoltaic cell/modules using bonobo optimizer," *Energies*, vol. 15, no. 1, p. 140, 2022, <https://doi.org/10.3390/en15010140>.
- [47] M. Naeijian, A. Rahimnejad, S. M. Ebrahimi, N. Pourmousa, and S. A. Gadsden, "Parameter estimation of PV solar cells and modules using Whippy Harris Hawks Optimization Algorithm," *Energy Reports*, vol. 7, pp. 4047-4063, 2021, <https://doi.org/10.1016/j.egy.2021.06.085>.
- [48] P. P. Biswas, P. N. Suganthan, G. Wu, and G. A. J. Amaratunga, "Parameter estimation of solar cells using datasheet information with the application of an adaptive differential evolution algorithm," *Renewable Energy*, vol. 132, pp. 425-438, 2019, <https://doi.org/10.1016/j.renene.2018.07.152>.
- [49] J. P. Ram, D. S. Pillai, N. Rajasekar, and V. K. Chinnaiyan, "Flower pollination based solar PV parameter extraction for double diode model," *Intelligent Computing Techniques for Smart Energy Systems*, vol. 607, pp. 303-312, 2020, [https://doi.org/10.1007/978-981-15-0214-9\\_34](https://doi.org/10.1007/978-981-15-0214-9_34).
- [50] M. Premkumar, P. Jangir, C. Ramakrishnan, G. Nalinipriya, H. H. Alhelou and B. S. Kumar, "Identification of Solar Photovoltaic Model Parameters Using an Improved Gradient-Based Optimization Algorithm With Chaotic Drifts," *IEEE Access*, vol. 9, pp. 62347-62379, 2021, <https://doi.org/10.1109/ACCESS.2021.3073821>.
- [51] B. Javidy, A. Hatamlou, and S. Mirjalili, "Ions motion algorithm for solving optimization problems," *Applied Soft Computing*, vol. 32, pp. 72-79, 2015, <https://doi.org/10.1016/j.asoc.2015.03.035>.
- [52] M. Awad, M. M. Mahmoud, Z. M. S. Elbarbary, L. Mohamed Ali, S. N. Fahmy, and A. I. Omar, "Design and analysis of photovoltaic/wind operations at MPPT for hydrogen production using a PEM electrolyzer: Towards innovations in green technology," *PLoS One*, vol. 18, no. 7, p. e0287772, 2023, <https://doi.org/10.1371/journal.pone.0287772>.
- [53] M. N. A. Hamid *et al.*, "Adaptive Frequency Control of an Isolated Microgrids Implementing Different Recent Optimization Techniques," *International Journal of Robotics and Control Systems*, vol. 4, no. 3, pp. 1000-1012, 2024, <https://doi.org/10.31763/ijrcs.v4i3.1432>.
- [54] A. T. Hassan *et al.*, "Adaptive Load Frequency Control in Microgrids Considering PV Sources and EVs Impacts: Applications of Hybrid Sine Cosine Optimizer and Balloon Effect Identifier Algorithms," *International Journal of Robotics and Control Systems*, vol. 4, no. 2, pp. 941-957, 2024, <https://doi.org/10.31763/ijrcs.v4i2.1448>.
- [55] A. A. Mas'ud *et al.*, "A Quasi oppositional smell agent optimization and its levy flight variant: A PV/Wind/battery system optimization application," *Applied Soft Computing*, vol. 147, p. 110813, 2023, <https://doi.org/10.1016/j.asoc.2023.110813>.
- [56] S. R. K. Joga *et al.*, "Applications of tunable-Q factor wavelet transform and AdaBoost classifier for identification of high impedance faults: Towards the reliability of electrical distribution systems," *Energy Exploration & Exploitation*, 2024, <https://doi.org/10.1177/01445987241260949>.
- [57] A. A. Elfatah, F. A. Hashim, R. R. Mostafa, H. A. El-Sattar, and S. Kamel, "Energy management of hybrid PV/diesel/battery systems: A modified flow direction algorithm for optimal sizing design — A case study in Luxor, Egypt," *Renewable Energy*, vol. 218, p. 119333, 2023,

<https://doi.org/10.1016/j.renene.2023.119333>.

- [58] Q. Niu, L. Zhang, and K. Li, "A biogeography-based optimization algorithm with mutation strategies for model parameter estimation of solar and fuel cells," *Energy Conversion and Management*, vol. 86, pp. 1173-1185, 2014, <https://doi.org/10.1016/j.enconman.2014.06.026>.
- [59] V. Lo Brano, A. Orioli, and G. Ciulla, "On the experimental validation of an improved five-parameter model for silicon photovoltaic modules," *Solar Energy Materials and Solar Cells*, vol. 105, pp. 27-39, 2012, <https://doi.org/10.1016/j.solmat.2012.05.028>.